Unified Elastic Modulus Characteristic Curve Equation for Variably Saturated Soils

Chao Zhang, A.M.ASCE[1]; Shaojie Hu, S.M.ASCE[2]; and Ning Lu, F.ASCE[3]

Abstract: A soil's elastic modulus is a fundamental property defining the soil's reversible stress-strain relation under mechanical and environmental loadings. It has been observed that a soil's elastic modulus can increase up to several orders of magnitude from fully saturated to dry conditions due to two distinct soil water retention mechanisms: adsorption and capillarity. Adsorption affects interparticle stress through van der Waals and electrostatic attraction and interparticle friction coefficient through water film retained by soil sorptive potential. Capillarity governs interparticle stress through capillary pressure and surface tension. The onset and scaling laws of the two mechanisms depend on the soil properties of specific surface area, pore-size distribution, cation exchange capacity, and soil mineralogy. These mechanisms are unified by a proposed elastic modulus characteristic curve (EMCC) equation. It is demonstrated that the proposed EMCC equation can well describe the moisture-dependent elastic modulus of a wide array of soils. Further, an interrelation among the EMCC equation, suction stress and soil shrinkage curves is established, which can greatly facilitate predicting suction stress from soil shrinkage curves and vice versa, further validating the EMCC equation in capturing soil's hydromechanical behavior. The practical importance of the EMCC equation is demonstrated through prediction of ground heave of various soils due to a hypothetical flooding event. **DOI: 10.1061/(ASCE)GT.1943-5606.0002718.**

Author keywords: Elastic modulus; Resilient modulus; Unsaturated soils; Soil sorptive potential; Matric potential; Capillarity; Adsorption; Soil shrinkage; Suction stress.

Introduction

Elastic modulus at finite strain (~ a few %) is a fundamental soil property describing soil deformation induced by mechanical and environmental loadings. It has been widely observed that the elastic modulus of a soil not only depends on a soil's mineralogy, fabrics, and compaction state but also heavily on the ambient humidity or soil water potential (e.g., Mancuso et al. 2002; Sawangsuriya et al. 2009; Schuettpelz et al. 2010; Khosravi and McCartney 2011; Ng et al. 2013; Lu and Kaya 2014; Han and Vanapalli 2016; Dong and Lu 2017; Dong et al. 2018; Banerjee et al. 2020). Such dependence can alter the soil's elastic modulus from hundreds of kPa to thousands of kPa for clayey soils (e.g., Sawangsuriya et al. 2009; Lu and Kaya 2013, 2014; Lu 2018). This variation in soil's elastic modulus is a critical constitutive relation underpinning the drying or wetting-induced deformations of earth and earthen structure systems. Therefore, how to accurately capture the dependence of soil's elastic modulus on water potential is critical to better understand and engineering geotechnical infrastructures in facing climate change, novel energy exploitation, and resource recovery, e.g., underground pipelines for conveying water and energy, dams for generating hydropower, subsea constructions for exploring offshore oil and gas resources, and beneficial reuse of industrial waste in embankment (e.g., Poulos 1995; Culligan et al. 2019).

Dependence of soil's elastic modulus on soil water potential stems from soil-water interaction. The energy levels of soil-water interaction mechanisms highly depend on soil mineralogy, specific surface area, cation exchange capacity, and pore-size distribution (e.g., Zhang and Lu 2018; Lu and Zhang 2019). Consequently, the soil's elastic modulus's dependence on soil water potential significantly varies with soil types. For example, the elastic modulus of silty and clayey soil is highly sensitive to the energy level of soil-water interaction, i.e., increasing up to dozens of times from zero water potential to the lowest water potential of several negative gigapascals (e.g., Lu and Kaya 2013; Zhang et al. 2017; Zhang and Lu 2018), whereas the elastic modulus of sandy soil only exhibits marginal dependence on water content. Yet it remains challenging in how to effectively quantify the role of soil-water interaction in changing soil's elastic modulus.

The soil-water interaction mechanisms include capillarity, multilayer adsorption, surface hydration, interlamellar cation hydration, and ion hydration with varying energy levels down to −2.0 GPa (Zhang et al. 2017). These mechanisms all unfailingly lower the free energy of soil water and contribute to soil's capacity in retaining water. Yet the origins of these mechanisms are distinct by two physically different forms: the first (capillarity) roots in internal mechanical interaction among soil water molecules, whereas the remaining mechanisms root in the electromagnetic interaction of soil water with external matters (soil solid). As such, these mechanisms can be further classified into two categories: the first is capillarity; the rest is adsorption. Recently, a definition of matric suction (ψ_m) unifying both adsorption and capillarity is proposed as (Lu and Zhang 2019; Zhang and Lu 2019b, 2020a):

[1]Professor, Ministry of Education Key Laboratory of Building Safety and Energy Efficiency, College of Civil Engineering, Hunan Univ., Changsha 410082, China (corresponding author). ORCID: https://orcid.org/0000-0002-6675-3940. Email: chao_zhang@hnu.edu.cn

[2]Ph.D. Student, Ministry of Education Key Laboratory of Building Safety and Energy Efficiency, College of Civil Engineering, Hunan Univ., Changsha 410082, China. ORCID: https://orcid.org/0000-0003-2730-930X. Email: sjhu@hnu.edu.cn

[3]Professor, Dept. of Civil and Environmental Engineering, Colorado School of Mines, 1012 14th St., Golden, CO 80401. Email: ninglu@mines.edu

Note. This manuscript was submitted on April 15, 2021; approved on September 15, 2021; published online on October 21, 2021. Discussion period open until March 21, 2022; separate discussions must be submitted for individual papers. This paper is part of the ***Journal of Geotechnical and Geoenvironmental Engineering***, © ASCE, ISSN 1090-0241.

$$\psi_m(w) = u_a - u_w(x, w) - \psi_{\text{sorp}}(x) \quad (1)$$

where w = gravimetric water content (g/g); u_a = ambient pressure (kPa); u_w = pore water pressure (kPa); x = statistical distance to particle surface (m); and ψ_{sorp} = soil sorptive potential (kPa). Soil sorptive potential (SSP) is the free energy change per unit volume of soil water due to its interaction with external matters. Albeit both decreasing the free energy of soil water, adsorption, and capillarity oppositely alter certain physical properties of soil water (Lu and Zhang 2019; Zhang and Lu 2020a), i.e., adsorption increases pore water pressure and soil water density, whereas capillarity decreases pore water pressure and soil water density (Zhang and Lu 2018).

To date, it remains unclear why and how adsorption and capillarity change soil's elastic modulus. To fill this knowledge gap, the writers will: (1) synthesize microscale mechanisms of dependence of soils' elastic modulus on water content, (2) develop a conceptual model for quantifying effects of adsorption and capillarity on elastic modulus, (3) establish a unified elastic modulus characteristic curve (EMCC) model for variably saturated soil, and (4) explore interrelations among elastic modulus, suction stress, and soil shrinkage curves.

Soil-Water Interaction Mechanisms for Changing Elastic Modulus

Soil's elastic modulus codifies a soil skeleton's ability in resisting deformation under loadings. This resistance at the bulk macroscale is dictated by the shear resistance among soil particles at the microscale, exclusively determined by two microscale variables, i.e., interparticle stress σ_{int} (kPa) and interparticle friction coefficient μ, as illustrated in Fig. 1. Here, the interparticle stress is defined as the statistically averaged contact mechanical and physicochemical stress among soil particles; the interparticle friction coefficient is defined as the statistically averaged friction coefficient, i.e., the ratio of interparticle normal and frictional stresses. Generally, an increase in these two variables produces an increase in microscale shear resistances and thereby an increase in soil's elastic modulus. Therefore, a soil's elastic modulus can be quantified by delineating how soil-water interaction affects the two microscale variables. Herein, the two microscale variables governing the EMCC and their dependence on soil-water interaction will be synthesized, yielding a conceptual model for the EMCC of soil.

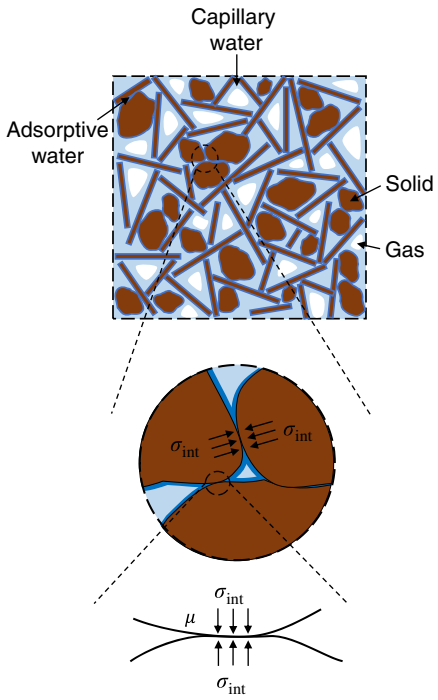

Fig. 1. Conceptual illustration of microscale variables determining soil's elastic modulus: interparticle force σ_{int} and interparticle friction coefficient μ.

Interparticle Stress

The stress state is one of the controlling factors determining the elastic moduli of saturated and dry soils. Specifically, an increase in interparticle stress or effective stress will increase the elastic modulus (e.g., Chang et al. 1989; Makse et al. 1999; Lu and Kaya 2014). Such dependence can be interpreted as the effect of interparticle friction. The higher interparticle stress suggests a more compacted soil skeleton, thereby more contact points and higher interparticle friction stress. Apparently, the increasing interparticle friction stress enhances the shear resistance of soils, thereby increasing soil's elastic modulus.

Suction stress is the effective stress produced by soil-water interaction, encapsulating soil-water interaction's effects on soil stress states (Lu and Likos 2006; Lu 2008). Suction stress consists of adsorptive suction stress and capillary suction stress (Lu and Likos 2006; Zhang and Lu 2020b). Suction stress varies with water content, yielding a characteristic curve called suction stress characteristic curve (SSCC) (Lu and Likos 2004). The behavior of SSCC heavily depends on fundamental soil properties such as cation exchange capacity, specific surface area, soil mineralogy, pore-size distribution, and compaction state. The adsorptive component of SSCC is generally an increasing (becoming less negative) function of water content because adsorptive water tends to penetrate the interparticle space and leads to a rapid decay of the van der Waals and electrostatic attraction between soil particles (Zhang and Lu 2020b). The capillary component of SSCC depends on the soil's pore-size distribution, soil water cavitation, and soil compaction history, first decreasing (becomes more negative) then increasing with increasing water content.

The interparticle stress in soil is exclusively contributed by suction stress under zero external stress conditions. The suction stress can be scaled to the interparticle stress with a statistically averaged contact area per unit cross-section area in soil. That is, the interparticle stress is proportional to the suction stress for a given soil structure and fabric. It is inferred that the interparticle stress variation with water content follows the patterns of SSCC shown in Fig. 2(a).

Interparticle Friction Coefficient

A soil's elastic modulus increases with increasing interparticle frictional stress, as elaborated in the preceding subsection. The interparticle frictional stress is associated with not only the interparticle stress but also the interparticle friction coefficient. Under the same interparticle stress σ_{int}, the higher the interparticle friction coefficient μ, the higher the shear resistance.

The interparticle friction coefficient is dictated by surface asperities and lubrication. In soils, the lubrication is exclusively provided by the water film coating soil particles. The thickness of such water film is determined by the magnitude of SSP (Lu and Zhang 2019; Zhang and Lu 2020a). Upon wetting, a soil's SSP will gradually convert to mechanical form in terms of pore water pressure and attract water molecules into the interparticle contact area. Such increasing retained water will lubricate the interparticle contact and

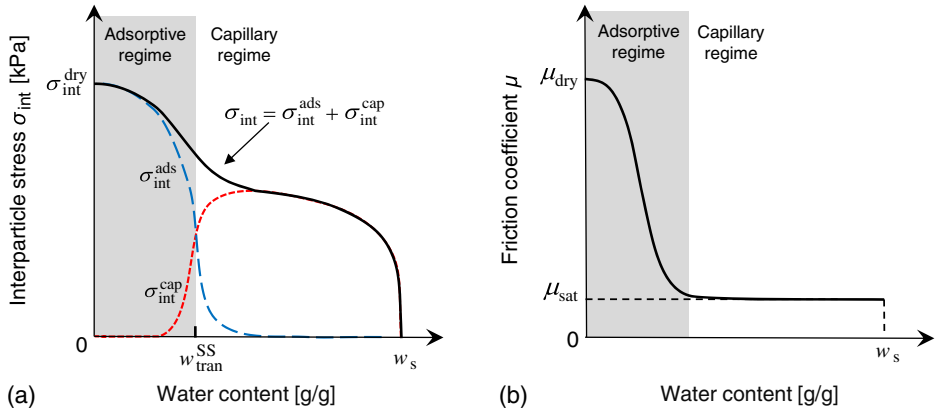

Fig. 2. Conceptual illustration of variation of microscale variables with water content: (a) interparticle stress; and (b) interparticle friction coefficient.

consequently reduce the interparticle friction coefficient. This reduction effect will reach its maximum when the interparticle contact area is fully covered with water. That is, the interparticle friction coefficient remains a constant beyond a certain water content. Thus, the interparticle friction coefficient decreases with increasing water content in the adsorptive regime and remains unchanged in the capillary regime ($\sim\mu_{sat}$), as conceptually illustrated in Fig. 2(b).

Conceptual Model

Soils' elastic modulus can be expressed in terms of an increasing function of the interparticle stress σ_{int} and interparticle friction coefficient μ. Hence, the elastic modulus's variation with water content of a soil (E) can be conceptually expressed as:

$$E(w) = f[\sigma_{int}(w), \mu(w)] \tag{2}$$

where σ_{int} = interparticle stress (kPa); and μ = interparticle friction coefficient (dimensionless).

Eq. (2) yields a conceptual model of EMCC of variably saturated soil, shown in Fig. 3. The EMCC can be explicitly separated into two branches: adsorptive EMCC and capillary EMCC. At the oven-dry state, soil particles hold the largest σ_{int} and μ, yielding the maximum of adsorptive EMCC. Upon wetting, adsorptive water gradually fills up interparticle contact space, thereby increasing interparticle distance and dielectric constant, both of which decrease interparticle contact stress σ_{int} (e.g., Israelachvili 2011; Butt and Kappl 2018; Zhang and Lu 2020b). Besides, adsorptive water coats the particle surface and lubricates interparticle contact, reducing interparticle friction coefficient μ. Both the decreased interparticle stress and reduced interparticle friction coefficient will decrease the elastic modulus of soil. Consequently, the adsorptive EMCC generally decays rapidly with increasing water content, shown in Fig. 3.

The variation of capillary EMCC is fully contributed by the capillary force among soil particles (e.g., Lu and Likos 2004). The magnitude of capillary force in soil is determined by the amount of capillary water content and curvature of water meniscus. At the dry end (low water content), there exists no capillary water in soil due to cavitation. Beyond the cavitation potential (e.g., Or and Tuller 2002; Lu 2016), capillary condensation occurs. With increasing water content, capillary water content increases, whereas the curvature of the menisci decreases. Such a unique changing pattern of water meniscus suggests that the capillary force first increases then decreases with water content. Because the capillary force contributes to interparticle stress in the capillary regime, the capillary EMCC demonstrates a nonmonotonic function of water content, shown in Fig. 3.

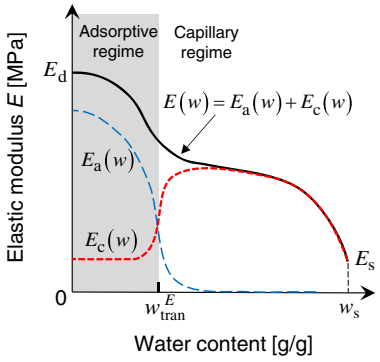

Fig. 3. Conceptual illustration of the proposed unified elastic modulus characteristic curve equation.

Development of the Proposed EMCC Model

The conceptual model above suggests that the EMCC equation can be explicitly divided into two hardening components, namely adsorptive EMCC (E_a) and capillary EMCC (E_c) (Lu 2018):

$$E(w) = E_a(w) + E_c(w) \tag{3}$$

Proposed Adsorptive Model

The proposed conceptual model shows that the soil's adsorptive elastic modulus maintains the maximum at the dry end and nonlinearly decays with increasing water content. The maximum adsorptive elastic modulus E_{am} equals the difference between elastic modulus at the oven-dry state and the saturated state

$$E_{am} = E_d - E_s \tag{4}$$

where E_d = elastic modulus at the oven-dry state (kPa); and E_s = elastic modulus at the saturated state (kPa). The magnitude of E_{am} is a function of soil properties of mineralogy and fabrics (pore structure distribution). Generally, a soil consisting of minerals yielding strong particle-particle van der Waals attraction and fabrics producing large contact area tends to exhibit a large value of

maximum adsorptive elastic modulus E_{am}. The nonlinear decay of adsorptive elastic modulus can be depicted by two factors, i.e., decay rate and ending point. The ending point of decay marks the diminishing of adsorptive elastic modulus, which can be determined by a characteristic water content called transitional water content from adsorption to capillarity (w^{E}_{tran}), as suggested by (Zhang and Lu 2020b). The decay rate highly depends on soil-water interaction mechanisms, and is represented by a dimensionless scaling function, following Zhang and Lu (2020b). Therefore, the adsorptive EMCC can be expressed as multiplying the maximum adsorptive elastic modulus ($E_{am} = E_d - E_s$) with a dimensionless scaling function $f_{ads}(w)$ ranging between 0 and 1:

$$f_{ads}(w) = \frac{1}{2}\left[1 - erf\left(\beta^{E}\frac{w - w^{E}_{tran}}{w^{E}_{tran}}\right)\right] \tag{5}$$

Accordingly, the adsorptive EMCC can be written as

$$E_a(w) = \frac{1}{2}\left[1 - erf\left(\beta^{E}\frac{w - w^{E}_{tran}}{w^{E}_{tran}}\right)\right](E_d - E_s) \tag{6}$$

where β^{E} = dimensionless parameter controlling the decay rate of adsorptive EMCC; and w^{E}_{tran} = transitional water content (g/g), symbolizing the transition from adsorption to capillarity. The dimensionless scaling function $f_{ads}(w)$ equals 1 at oven-dry state ($w = 0$ g/g), indicating the maximum adsorptive elastic modulus E_{am}, and decays to 0, suggesting the vanishment of the hardening in adsorptive elastic modulus.

Proposed Capillary Model

The proposed conceptual model suggests that the capillary EMCC is contributed by the interparticle capillary force, and the capillary EMCC's variation with water content follows the patterns of the capillary part of SSCC, i.e., first increasing then decreasing with water content. The capillary SSCC equation is well established and validated (Zhang and Lu 2020b) by multiplying the SSCC equation (Lu et al. 2010) with a dimensionless scaling function f_{cap}. The capillary EMCC equation can be written by the following capillary SSCC equation:

$$E_c(w) = E_s + (E_{cm} - E_s)\frac{w}{w_s}\left[\left(\frac{w}{w_s}\right)^{\frac{n^E}{1-n^E}} - 1\right]^{\frac{1}{n^E}} \tag{7}$$

where E_s = elastic modulus at saturated state (MPa); E_{cm} = maximum capillary elastic modulus (MPa); and n^{E} = fitting parameter related to the pore size distribution.

Eq. (7) predicts the soil's elastic modulus as a decreasing function of water content, in contrast with the generally nonmonotonic capillary elastic modulus shown in Fig. 3. This is because the cavitation phenomenon has not been previously included. The cavitation phenomenon imposes a lower physical limit for negative capillary pressure. Beyond this limit, capillary water will spontaneously evaporate (e.g., Or and Tuller 2002; Lu and Likos 2004; Baker and Frydman 2009), and all the soil water will be exclusively adsorptive water, indicating the reduction of capillary elastic modulus to E_s. Herein, a dimensionless scaling function $f_{cap}(w)$ ranging between 1 and 0 is introduced to capture the cavitation effects on capillarity elastic modulus, which can be expressed as

$$f_{cap}(w) = \frac{1}{2}\left[1 + erf\left(3\frac{w - w^{E}_{tran}}{w^{E}_{tran}}\right)\right] \tag{8}$$

Thus, capillary hardening [Eq. (7)] can be extended by multiplying the scaling function Eq. (8) as:

$$E_c(w) = \frac{1}{2}\left[1 + erf\left(3\frac{w - w^{E}_{tran}}{w^{E}_{tran}}\right)\right]\left\{E_{cm}\frac{w}{w_s}\left[\left(\frac{w}{w_s}\right)^{\frac{n^E}{1-n^E}} - 1\right]^{\frac{1}{n^E}}\right\} + E_s \tag{9}$$

Proposed Elastic Modulus Function Variability

The proposed EMCC model [Eqs. (3), (6), and (9)] involves seven clearly defined physical parameters to unify the soil's elastic modulus variation with soil-water interaction: two for adsorption, β^{E} and E_d; four for capillarity, E_{cm}, E_s, w_s, and n^{E}; and one for both, w^{E}_{tran}, denoting the transition between adsorptive and capillary EMCCs. A series of parametric studies are conducted to assess the variability of the proposed EMCC model.

The dry-end elastic modulus (E_d) controls the magnitude of the total elastic modulus, illustrated in Fig. 4(a). Generally, E_d depends on soil mineralogy and fabrics, and can vary up to several MPa. The saturated elastic modulus (E_s) also demonstrates a strong variation with soil mineralogy and fabrics. Existing data (e.g., Lu and Kaya 2013) show that for sandy soils the dry-end elastic modulus is almost equal to the saturated elastic modulus, that is, sandy soil's elastic modulus is insensitive to water content. In contrast, the dry-end elastic modulus of silty and clayey soils is considerably much higher than their saturated elastic modulus, ranging in the order of 4–24 times.

The dimensionless parameter β^{E} dictates the decay rate of adsorptive elastic modulus, illustrated in Fig. 4(b). A lower value of β^{E} indicates that the adsorptive elastic modulus more slowly decays with water content. The value of β^{E} partly reflects a soil's adsorptive water retention capacity and is highly related to a soil's SSA. For expansive soils with large SSA (e.g., 668 m^2/g for Wyoming bentonite), the value of β^{E} falls within the range of 2.0–2.5, whereas for nonexpansive soils the value of β^{E} is approximately 2.5–3.0. To minimize the physical parameters, parameter β^{E} is fixed as 2.0 for soils with SSA > 140 m^2/g, and 3.0 for soils with SSA ≤ 140 m^2/g.

The parameter E_{cm} defines the magnitude of the capillary elastic modulus, illustrated in Fig. 5(a). A higher value of E_{cm} indicates a higher magnitude of capillary elastic modulus. It reflects the upper bound for capillarity hardening effects on soil's elastic modulus, thus is related to pore-size distribution.

The parameter n^{E} can be physically related to the pore-size distribution. It dictates the decay rate of the capillary elastic modulus with increasing water content, shown in Fig. 5(b). This decay occurs after reaching the maximum capillary elastic modulus. Generally, a lower value of n^{E} suggests a smaller decay rate, that is, the capillary elastic modulus is more persistent with increasing water content.

The parameter w^{E}_{tran} marks the boundary separating the regions where the adsorptive elastic modulus dominates and where capillary elastic modulus dominates, shown in Figs. 4(c) and 5(c). The parameter w^{E}_{tran} reflects the adsorptive water retention capacity of the soil, thus is highly related to the soil's SSA and cation exchange capacity. An expansive soil with high SSA and cation exchange capacity is expected to exhibit a high value of w^{E}_{tran}.

Assessments of the Unified EMCC Equation

Experimental Dataset

An experimental dataset of eight soils from the literature has been collected to validate the proposed EMCC equation. The dataset consists of two sandy soils (Esperance sand and Ottawa sand),

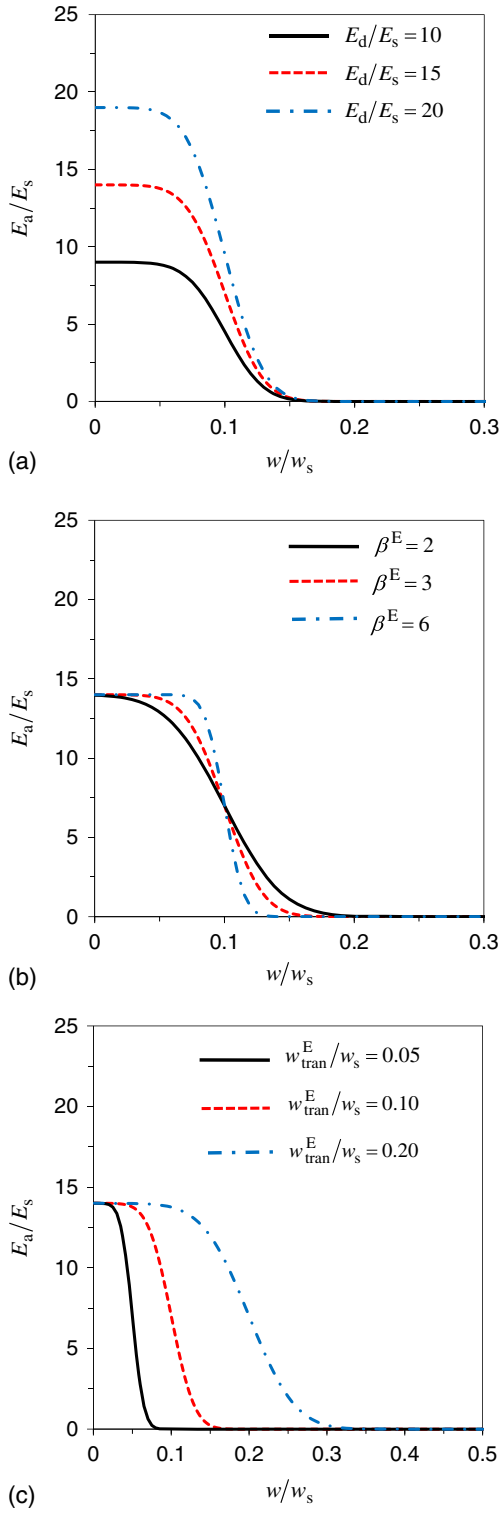

Fig. 4. Variability of the proposed adsorptive elastic modulus equation with: (a) the ratio of dry elastic modulus to the saturated elastic modulus E_d/E_s; (b) the parameter β^E; and (c) the ratio of transitional water content to saturated water content w^E_{tran}/w_s.

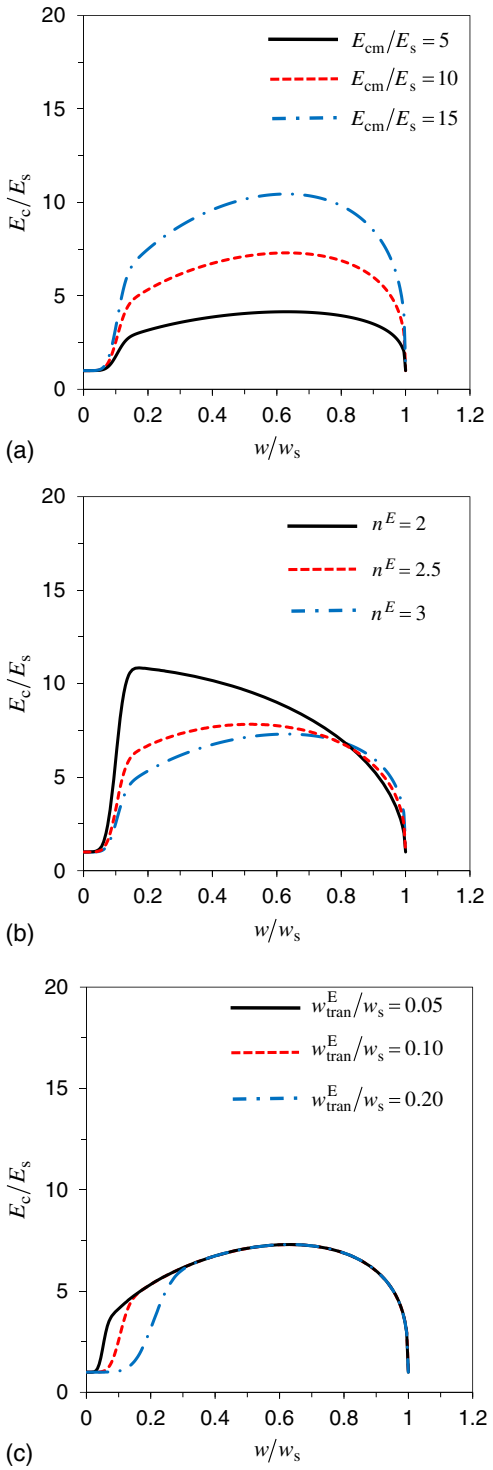

Fig. 5. Variability of the proposed capillary elastic modulus equation with: (a) the ratio of the maximum capillary elastic modulus to the elastic modulus at saturated state E_{cm}/E_s; (b) the fitting parameter n^E; and (c) the ratio of transitional water content to saturated water content w^E_{tran}/w_s.

two silty soils (Balt silt and Iowa silt), and four clayey soils (Georgia kaolinite, Denver claystone, Missouri clay, and Denver bentonite). The eight soils include a wide array of soil types ranging from non-expansive soils to high-expansive soils, thus is representative of general soil types. The EMCC data for Esperance sand and Georgia kaolinite are from Lu and Kaya (2013), and the other EMCC data are from Lu and Dong (2017). All the experimental data of the elastic modulus is obtained by the nondestructive drying cake method (Lu and Kaya 2013). This method employs an environmental chamber to monitor relative humidity (soil suction), a digital camera to record the deformation, a balance to record the weight of the soil cake, and an automatic loading system to conduct uniaxial

Table 1. Geotechnical index properties, soil classification, and source of the soil dataset

Soil	USCS	Expansive soil classification[a]	Porosity[b]	SSA (m^2/g)[c]	Specific gravity[b]	Atterberg limits[d] LL	PL	PI	Elastic modulus data source	Soil shrinkage data source	Experimental method of modulus[e]
Ottawa sand	SP	Nonexpansive	0.382	—	2.65	—	—	—	Lu and Dong (2017)	—	UK_0C
Esperance sand	SP	Nonexpansive	0.418	—	2.65	—	—	—	Lu and Kaya (2013)	—	UK_0C
Balt silt	ML	Low-expansive	0.458	91	2.72	27	21	6	Lu and Dong (2017)	Lu and Dong (2017)	UUC
Iowa silt	ML	Low-expansive	0.492	110	2.70	34	23	11	Lu and Dong (2017)	Lu and Dong (2017)	UUC
Georgia kaolinite	MH	Nonexpansive	0.522	31	2.66	44	26	18	Lu and Kaya (2013)	—	UUC
Denver claystone	CL	Expansive	0.471	145	2.70	44	23	21	Lu and Dong (2017)	Lu and Dong (2017)	UUC
Missouri clay	CL	Expansive	0.490	—	2.67	36	17	19	Lu and Dong (2017)	Lu and Dong (2017)	UUC
Denver bentonite	CH	High-expansive	0.692	668	2.70	118	45	73	Lu and Dong (2017)	Lu and Dong (2017)	UUC

[a]According to the method by McKeen (1992).
[b]Lu (2018).
[c]Akin and Likos (2014).
[d]Lu and Kaya (2014).
[e]UK_0C denotes the uniaxial K_0 compression test, and UUC represents the uniaxial unconfined compression test.

unconfined compression tests for fine-grained soils or the uniaxial K_0 compression test for coarse-grained soils to measure the elastic modulus (Lu and Kaya 2013; Dong and Lu 2017). Table 1 summarizes the geotechnical engineering properties and references of the selected soil dataset.

Performance of the Proposed Equation

A least-squares method is chosen to fit the proposed EMCC equation [defined by Eqs. (3), (6), and (9)] with the experimental elastic modulus dataset. Best fitting parameters are summarized in Table 2. The proposed unified EMCC equation unfailingly excellently matches with the experimental data with a coefficient of determination R^2 value higher than 0.96 for silty and clayey soils, 0.65 for sandy soils, illustrated in Figs. 6 and 7.

The two sandy soils' elastic modulus only shows marginal dependence on water content, shown in Figs. 6(a and b). This is consistent with the experimental observations of sandy soils' relatively weak soil-water interaction by adsorption (e.g., Lu 2016). This adsorptive hardening can be interpreted as a result of the adsorptive film water's lubrication effects. That is, adsorptive water film coating sandy soils' particles tends to lubricate the interparticle contact thereby slightly decreases the soil's elastic modulus, demonstrated in Fig. 2(b). Additionally, the unified EMCC equation predicts that the sandy soils exhibit low w^{E}_{tran} values (0.024 g/g for Ottawa sand and 0.043 g/g for Esperance sand), showing consistency with their soil water retention curves (Lu 2016).

The two silty soils' elastic moduli vary up to five times from their saturated state to oven-dry state, shown in Figs. 6(c and d). This nonlinear variation can be excellently captured by the proposed EMCC equation, e.g., $R^2 = 0.99$ for Balt silt and $R^2 = 1.00$ for Iowa silt. The transitional water content values are predicted to be 0.040 for Balt silt, and 0.091 for Iowa silt. Below this unique water content value, the elastic modulus variation is dominatingly contributed by adsorption. The adsorption can vary the Balt silt's elastic modulus from 2.4 to 2.6 MPa, and the Iowa silt's elastic modulus from 2.0 to 3.1 MPa. Beyond the transitional water content, capillarity plays a dominating role in changing soil's elastic modulus, e.g., varying the Balt silt's elastic modulus from 2.4 to 0.5 MPa, and the Iowa silt's elastic modulus from 2.0 to 0.7 MPa.

For the nonexpansive clay, the EMCC of Georgia kaolinite follows a similar pattern with that of sandy soils, i.e., first decreasing, then increasing, and then decreasing with increasing water content, shown in Fig. 7(a). This unique pattern can be fully described by the proposed EMCC equation with $R^2 = 0.96$. This pattern stems from the mineralogy of Georgia kaolinite where 1:1 mineral prevails, leading to the weak adsorption on internal surface. The internal surface area includes both the area of interparticle contact and interlamellar contact at the oven-dry state (Lu and Zhang 2020). A lamella of kaolinite refers to a crystalline layer consisting of a silica sheet and an octahedral sheet, and a particle of kaolinite is an aggregate consisting of a stack of lamellas (e.g., Mitchell and Soga 2005). Therefore, the interlamellar contact area is the area shared by two adjacent crystalline layers, whereas the interparticle contact area is the area shared by two adjacent aggregates. For Georgia kaolinite, adsorptive water only resides on the external surface and interparticle contact area, whereas the interlamellar contact area is inaccessible for water adsorption (Zhang and Lu 2019a). Therefore, adsorption is relatively weak for Georgia kaolinite, showing accordance with a moderate $w^{E}_{tran} = 0.069$ g/g predicted

Table 2. Parameters for the proposed equation and power law equation

Soil	w_s (g/g)	Proposed EMCC E_d (MPa)	E_{cm} (MPa)	E_s (g/g)	n^E	w^{E}_{tran} (g/g)	α	Power law E_d (MPa)	E_s (MPa)	m_{pl}
Ottawa sand	0.234	2.980	0	2.883	1.941	0.024	3.0	2.980	2.883	5.000
Esperance sand	0.250	3.371	0.036	3.093	3.000	0.043	3.0	3.428	3.087	0.291
Balt silt	0.310	2.568	1.263	0.462	1.804	0.040	3.0	2.569	0.462	1.523
Iowa silt	0.361	3.070	1.447	0.675	1.935	0.091	3.0	3.070	0.675	1.140
Georgia kaolinite	0.456	4.625	5.865	0.276	1.850	0.069	3.0	6.63	0.312	2.957
Denver claystone	0.328	2.512	1.511	0.200	1.918	0.096	2.0	2.512	0.200	1.644
Missouri clay	0.355	1.873	1.475	0.181	2.738	0.137	2.0	1.873	0.181	2.265
Denver bentonite	0.835	5.300	0.466	0.230	1.507	0.251	2.0	5.300	0.230	0.621

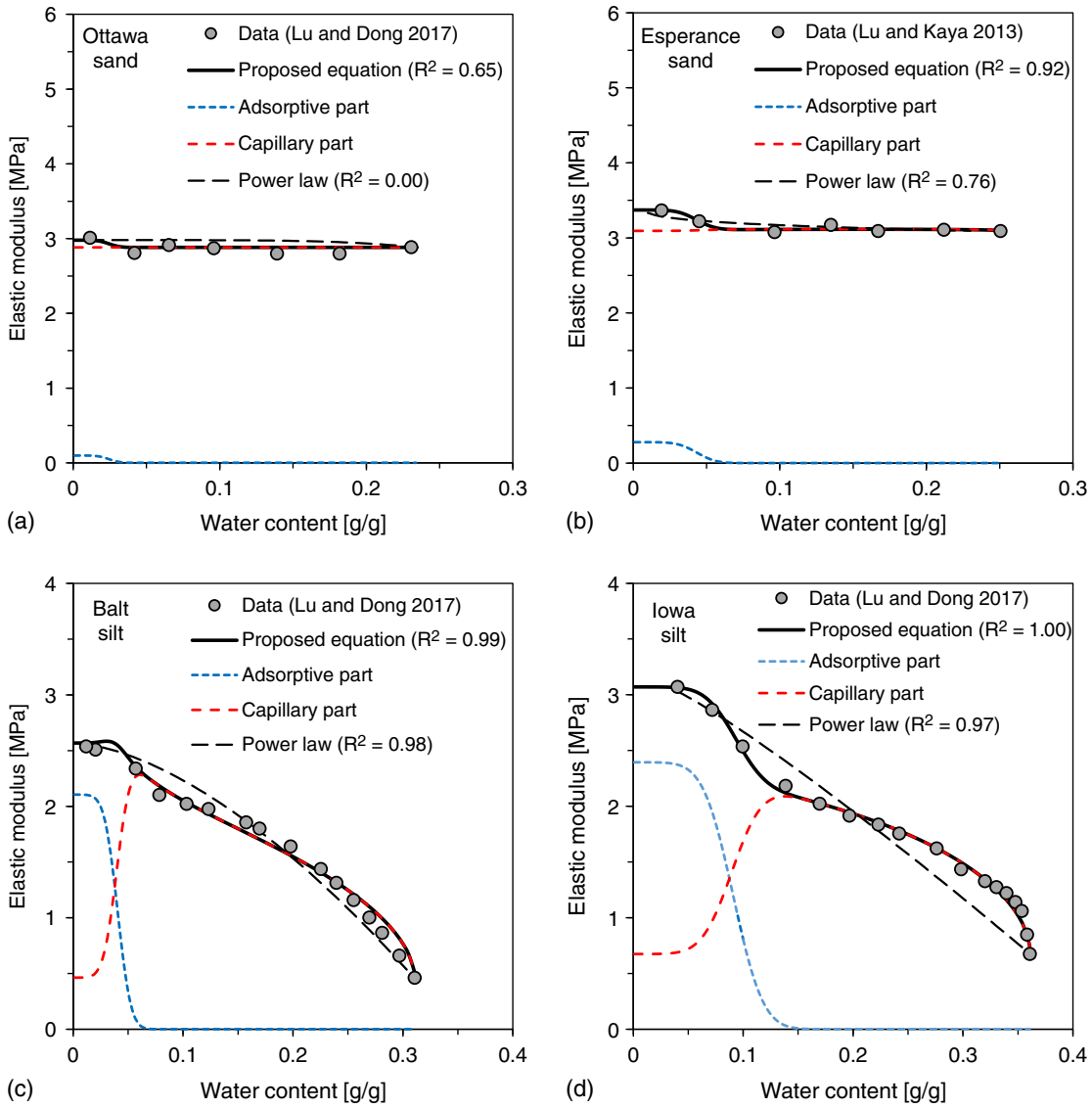

Fig. 6. Fitted unified elastic modulus function and the power law (Lu and Kaya 2014) with measured data for: (a) Ottawa sand; (b) Esperance sand; (c) Balt silt; and (d) Iowa silt.

by the proposed EMCC equation. In contrast, capillarity is strong due to its predominating fine particles. A weak adsorption indicates a relatively small magnitude of the maximum adsorptive elastic modulus E_{am} (4.0 MPa), whereas a strong capillarity leads to a relatively large magnitude of the maximum capillary elastic modulus E_{cm} (5.9 MPa), shown in Fig. 7(a). At the oven-dry state, the decreased capillary elastic modulus cannot be fully compensated by the increased adsorptive elastic modulus. Consequently, the peak of the total elastic modulus occurs at ~0.1 g/g water content rather than at the oven-dry state.

The three expansive clayey soils' elastic modulus demonstrates a strong variation in the adsorptive regime, e.g., from 2.5 to 1.6 MPa for Denver claystone, from 1.9 to 1.1 MPa for Missouri clay, and from 5.3 to 1.2 MPa for Denver bentonite, illustrated in Figs. 7(b–d). As shown, the proposed EMCC equation can excellently match the experimental data with $R^2 \geq 0.99$. The transitional water content predicted by the proposed EMCC equation for the three soils is much higher than silty and sandy soils, i.e., $w^{E}_{tran} = 0.096$ g/g for Denver claystone, $w^{E}_{tran} = 0.137$ g/g for Missouri clay, and $w^{E}_{tran} = 0.251$ g/g for Denver bentonite. These high values of transitional water content suggest the strong adsorptive water retention capacity of these soils in accordance with their high SSA values listed in Table 1.

The proposed EMCC model extends the power law (Lu and Kaya 2014) in terms of explicitly separating adsorptive and capillary elastic modulus and encapsulating the cavitation phenomenon. To quantitatively assess the proposed EMCC model over existing models, the power law is fitted to the experimental dataset for comparison. The best-fitting parameters are summarized in Table 2. Generally, the proposed EMCC model outperforms the power law in terms of fitting performance (R^2 value) and physical representation of adsorptive and capillary hardening. For sandy soils, the proposed EMCC model can capture the nonmonotonic variation of the modulus with water content, which cannot be described by the power law. Also, for Georgia kaolinite, the proposed EMCC model overcomes the inability of the power law in capturing the fluctuation of elastic modulus at low water content. For other clayey and silty soils, albeit that both the power law and the proposed EMCC model can describe the decreasing function of the elastic modulus of water content, the proposed EMCC model can closely

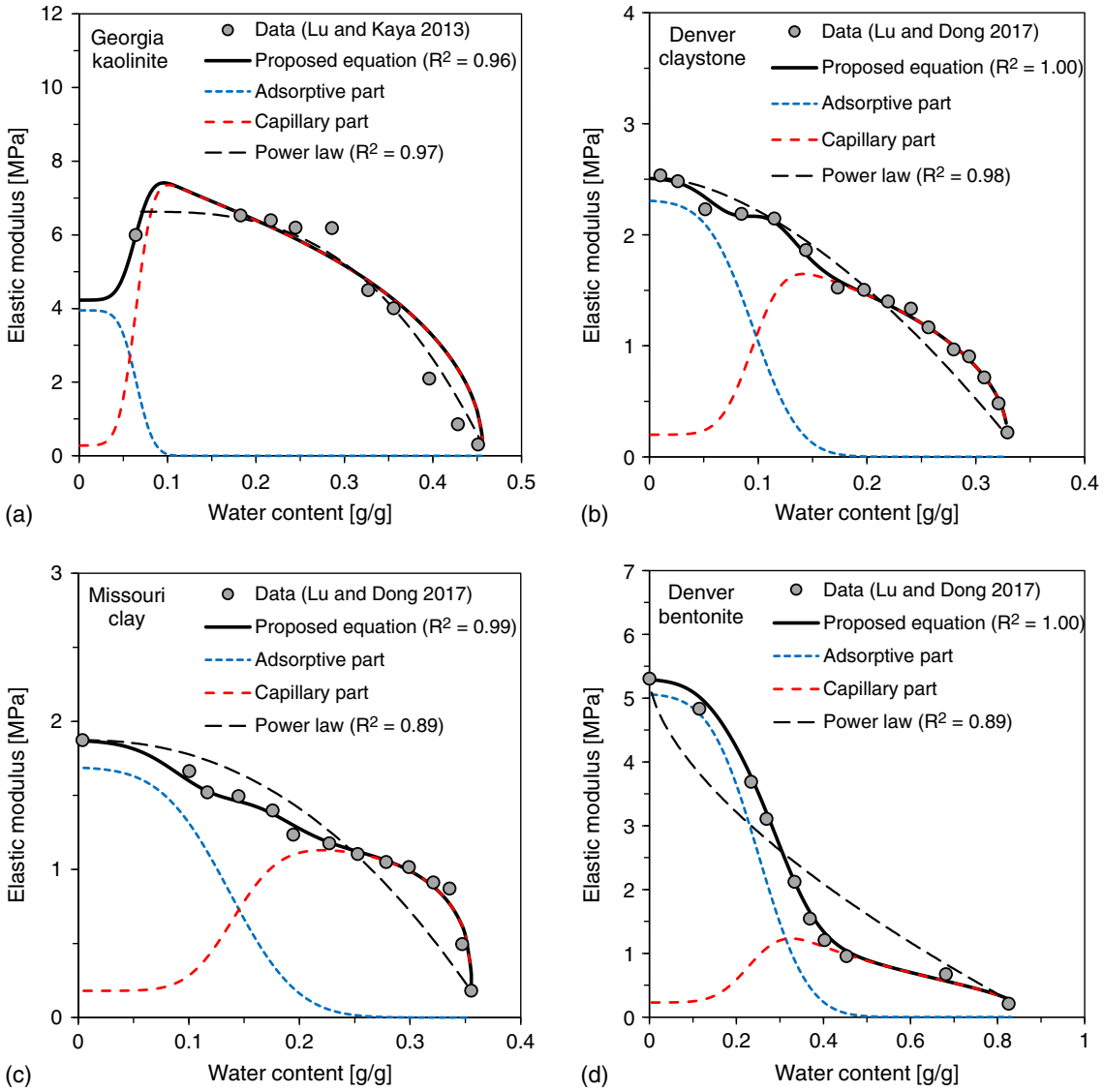

Fig. 7. Fitted unified elastic modulus function and the power law (Lu and Kaya 2014) with measured data for: (a) Georgia kaolinite; (b) Denver claystone; (c) Missouri clay; and (d) Denver bentonite.

represent the highly nonlinear decay of elastic modulus in terms of water content.

Interrelation among EMCC, SSCC, and Soil Shrinkage Curves

EMCC encodes soil-water interaction's impact on the elastic modulus, whereas SSCC delineates soil-water-interaction induced effective stress. That is, both EMCC and SSCC quantify how the soil-water interaction alters soil's mechanical properties due to adsorption and capillarity. It is therefore anticipated that EMCC and SSCC are intrinsically interrelated. Their interrelations can be well illustrated through soil shrinkage curves, the relation between the void ratio and water content (or moisture ratio). Soil shrinkage curves reflect the soil deformation induced by moisture changes or fundamentally by soil-water interaction. Specifically, with moisture varying, soil-water interaction varies soil effective stress (SSCC) and elastic modulus (EMCC) thereby results in soil shrinkage. As such, SSCC can be measured in terms of soil deformation under zero external loadings with EMCC, as proposed by Lu and Kaya (2013). In return, SSCC and EMCC can be utilized to estimate soil shrinkage curves, as suggested by Zhang and Lu (2020b). These interrelations will be demonstrated below.

Determining Suction Stress from EMCC and Soil Shrinkage Curves

The soil shrinkage curves can be measured by the drying cake method (Lu and Kaya 2013; Dong and Lu 2017). The drying cake method measures the soil shrinkage data at certain water content intervals. The corresponding suction stress change ($\Delta\sigma^s$) from water content w_1 to water content w_2 can be estimated from the following equation (see Appendix I for derivation):

$$\Delta\sigma^s = \frac{1}{3(1-2v)}\int_{w_1}^{w_2}\frac{E(w)}{1+e(w)}\frac{\mathrm{d}e}{\mathrm{d}w}\mathrm{d}w \tag{10}$$

where v = Poisson's ratio (0.25); and $e(w)$ = soil shrinkage curve function and is obtained through linear interpolation of measured soil shrinkage data. For example, the $e(w)$ between soil shrinkage

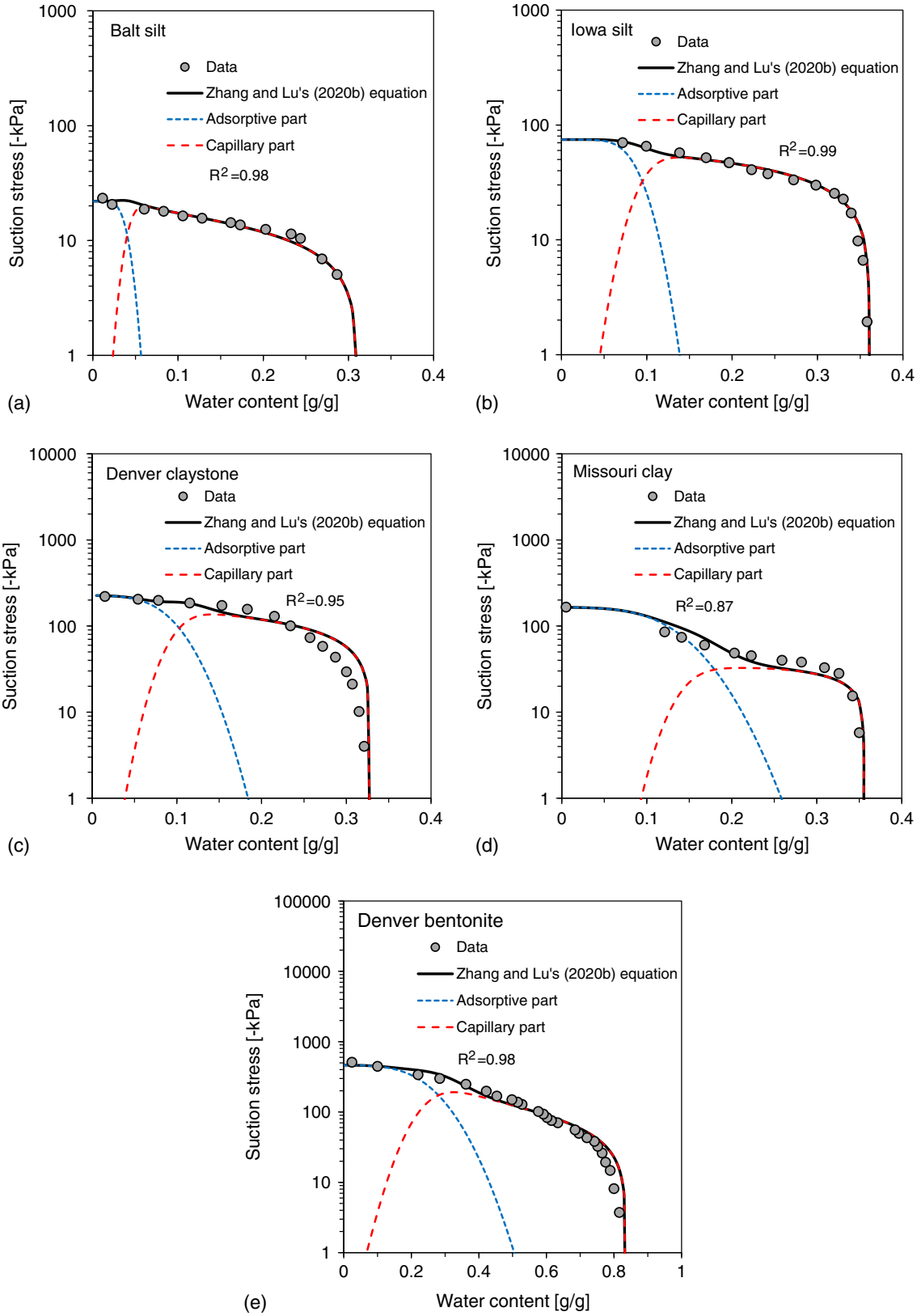

Fig. 8. Calculated suction stress data and fitted unified effective stress equation (Zhang and Lu 2020b) for: (a) Balt silt; (b) Iowa silt; (c) Denver claystone; (d) Missouri clay; and (e) Denver bentonite.

data points (w_1, e_1) and (w_2, e_2) can be written as $e(w) = e_2 + \frac{e_1 - e_2}{w_1 - w_2}(w - w_2)$.

Thus, suction stress values can be determined from soil shrinkage data through Eq. (10) with EMCC $[E(w)]$. The soil shrinkage data for two silty and three clayey soils in the previous section have been measured (Lu and Dong 2017) and are selected for determining suction stress. The proposed EMCC equation is adopted, and the corresponding parameters are selected from Table 2.

The determined suction stress data for the five soils is shown in Fig. 8. Silty soil suction stress data decreases upon drying, e.g., varying from 0 to −23.41 kPa for the Balt silt and from 0 to −71.53 kPa for the Iowa silt. Clayey soil suction stress data exhibit a more significant decrease upon drying and much lower (more negative) values near the dry-end, e.g., from 0 to −166.11 kPa for Missouri clay, and from 0 to −508.68 kPa for Denver bentonite.

Fitting Suction Stress Data with SSCC Equation

The suction stress variation is induced by the two soil-water interaction mechanisms, i.e., adsorption and capillarity. Such variation can be fully captured by the unified effective stress equation proposed by Zhang and Lu (2020b):

$$\sigma^s(w) = \sigma^s_{\text{ads}}(w) + \sigma^s_{\text{cap}}(w) \tag{11}$$

$$\sigma^s_{\text{ads}}(w) = \frac{1}{2}\left[1 - erf\left(\beta^{\text{SS}}\frac{w - w^{\text{SS}}_{\text{tran}}}{w^{\text{SS}}_{\text{tran}}}\right)\right]\sigma^s_{\text{dry}} \tag{12}$$

$$\sigma^s_{\text{cap}}(w) = \frac{1}{2}\left[1 + erf\left(3\frac{w - w^{\text{SS}}_{\text{tran}}}{w^{\text{SS}}_{\text{tran}}}\right)\right] \times \left\{-\frac{1}{\alpha^{\text{SS}}}\frac{w}{w_s}\left[\left(\frac{w}{w_s}\right)^{\frac{n^{\text{SS}}}{1-n^{\text{SS}}}} - 1\right]^{\frac{1}{n^{\text{SS}}}}\right\} \tag{13}$$

where σ^s_{ads} = adsorptive suction stress (kPa); σ^s_{cap} = capillary suction stress (kPa); σ^s_{dry} = suction stress at dry end (kPa); $w^{\text{SS}}_{\text{tran}}$ = transitional water content (g/g); β^{SS} = dimensionless parameter; α^{SS} = fitting parameter related to the inverse of the capillary suction stress (kPa^{-1}); w_s = saturated water content (g/g); and n^{SS} = fitting parameter related to the pore-size distribution.

The proposed EMCC equation [Eqs. (3), (6), and (9)] and the unified effective stress equation [Eqs. (11)–(13)] share three interrelated physical parameters, i.e., the transitional water content $w^{\text{SS}}_{\text{tran}}$ for suction stress and $w^{\text{E}}_{\text{tran}}$ for elastic modulus, the fitting parameter related to the pore-size distribution n^{SS} for suction stress, and n^{E} for elastic modulus, the dimensionless parameter controlling the decay rate of adsorptive suction stress β^{SS}, and adsorptive elastic modulus β^{E}. Both elastic modulus and suction stress quantify the soil-water interaction's impact on the soil skeleton's mechanical properties. Thus, it is anticipated that the three groups of interrelated parameters should be identical for the same soils.

The unified effective stress equation [Eqs. (11)–(13)] is used to fit the suction stress data by fixing $w^{\text{SS}}_{\text{tran}} = w^{\text{E}}_{\text{tran}}$, $n^{\text{SS}} = n^{\text{E}}$, and $\beta^{\text{SS}} = \beta^{\text{E}}$, shown in Fig. 8. The resulting best-fit parameters are summarized in Table 3. As shown, the unified effective stress equation can well represent suction stress data with $R^2 = 0.87$ for Missouri clay, and $R^2 \geq 0.95$ for the other four soils. The good fitting performance confirms the anticipated equivalence of the three interrelated parameters shared by the EMCC and the unified effective stress equation. Additionally, the equivalence of $w^{\text{SS}}_{\text{tran}}$ and $w^{\text{E}}_{\text{tran}}$ implies a linear relation between $w^{\text{E}}_{\text{tran}}$ and the maximum adsorptive water content ($w^{\text{SWR}}_{\text{amax}}$) in the Lu (2016) SWRC model. The transitional water content for suction stress ($w^{\text{SS}}_{\text{tran}}$) has been shown to be proportional with ($w^{\text{SWR}}_{\text{amax}}$) with a ratio of ($w^{\text{SS}}_{\text{tran}}$) to ($w^{\text{SWR}}_{\text{amax}}$) as 1.55 (Zhang and Lu 2020b). Hence, it is anticipated that the ($w^{\text{E}}_{\text{tran}}$) predicted by the proposed EMCC equation is linearly correlated with the maximum adsorptive water content in Lu's SWRC model.

Table 3. Parameters for the unified effective stress equation

Soil	σ^s_{dry} (−kPa)	α^{SS} (kPa^{-1})	n^{SS}	β^{SS}	$w^{\text{SS}}_{\text{tran}}$ (g/g)
Balt silt	21.97	0.073	1.804	3.0	0.040
Iowa silt	74.49	0.019	1.935	3.0	0.091
Denver claystone	226.34	0.007	1.918	2.0	0.096
Missouri clay	165.10	0.020	2.738	2.0	0.137
Denver bentonite	464.63	0.011	1.507	2.0	0.251

Predicting Soil Shrinkage Curves with EMCC and SSCC

The EMCC and unified effective stress equation can be implemented to predict soil shrinkage curves through the following equation (see Appendix II for derivation):

$$e(w) = [e(w_0) + 1]\exp\left[\int_{w_0}^{w}\frac{3(2v-1)}{E(w)}\frac{\mathrm{d}\sigma^s}{\mathrm{d}w}\mathrm{d}w\right] - 1 \tag{14}$$

where e_0 = initial void ratio; and w_0 = initial water content (g/g), generally equal to saturated water content w_s.

Substituting the unified EMCC [Eqs. (3), (6), and (9)] and effective stress equations [Eqs. (11)–(13)] into Eq. (14) yields soil shrinkage curves. The predicted soil shrinkage curves generally match well with the measured data from Lu and Dong (2017), shown in Fig. 9, with $R^2 \geq 0.97$ for the Balt silt, Iowa silt, and Denver bentonite, and $R^2 = 0.90$ for the Missouri clay and Denver bentonite. This confirms the capability of Eq. (14) with the unified EMCC and effective stress equations in predicting soil shrinkage curves, further substantiating the proposed EMCC model's ability in capturing the impact of adsorption and capillarity on the elastic modulus.

Practical Significance of Elastic Modulus Variation under Field Conditions

The elastic modulus of soil is one of the most fundamental soil properties underlying various geotechnical engineering problems, such as foundation settlement, slope stability, and swelling heave. Recently, global climate change poses new uncertainties to infrastructure safety, e.g., disturbing subsurface moisture distribution. Thereby, it is imperative to quantitively assess the mechanical status of geotechnical infrastructures under perturbated moisture conditions, considering accurate modeling of soil's elastic modulus. Here, the writers use a problem of estimating a soil layer's heave due to flooding to illustrate the significance of capturing elastic modulus variation.

A flat homogeneous soil layer with a thickness of h_0 is considered. The water table is set at the bottom of the soil layer. The upper boundary of the soil layer is set hydrologically as a steady evaporation with a flux of q (6.34×10^{-8} m/s). At the steady evaporation state, i.e., $q > 0$, the water content and matric suction profiles can be obtained analytically (Lu and Likos 2004), illustrated in Fig. 10(a). Detailed mathematical description is presented in Appendix III. At the steady state, water content increases nonlinearly with depth, and matric suction decreases linearly with depth. Using the analytical profiles of water content and matric suction, the elastic modulus and suction stress profiles can be calculated with the proposed EMCC equation and unified effective stress equation, shown in Fig. 10(a).

Suppose a severe tropical storm with a 200-mm rainfall occurred within several days so that the top 0.5 m of the soil layer becomes fully saturated during the flooding, the resulting water content

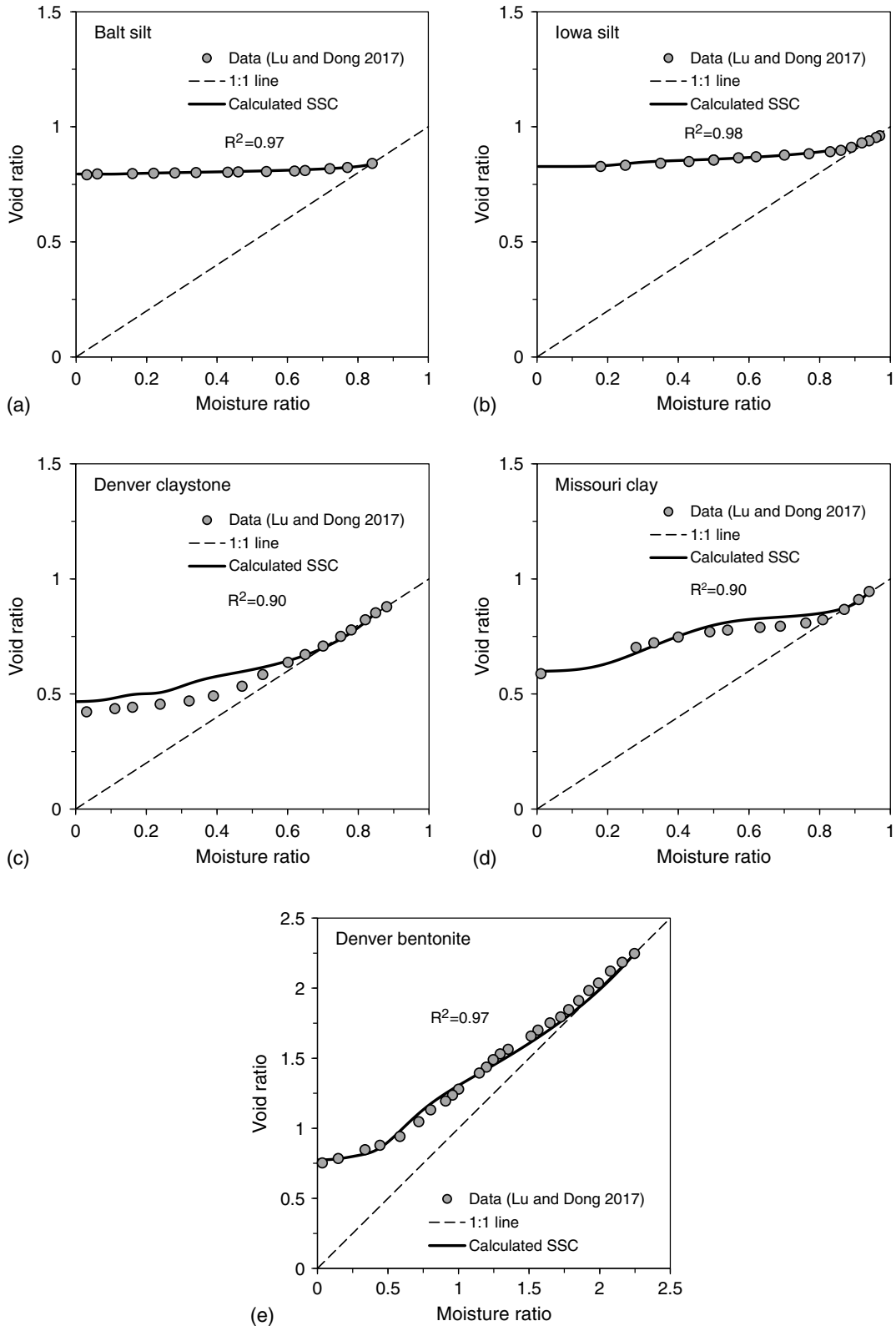

Fig. 9. Predicted soil shrinkage curves using the proposed EMCC equation and the unified effective stress equation for: (a) Balt silt; (b) Iowa silt; (c) Denver claystone; (d) Missouri clay; and (e) Denver bentonite.

[Eq. (22)], matric suction [Eq. (23)], suction stress [Eqs. (11)–(13)], and elastic modulus [Eqs. (3), (6), and (9)] profiles are calculated and shown in Fig. 10(b). The top 0.5 m of the soil layer is fully saturated, and the suction stress and elastic modulus profiles can remarkably change, resulting in a heave or settlement at the ground surface. The ground heave or settlement Δh can be calculated through the changes in suction stress and elastic modulus as follows (see Appendix III for derivation):

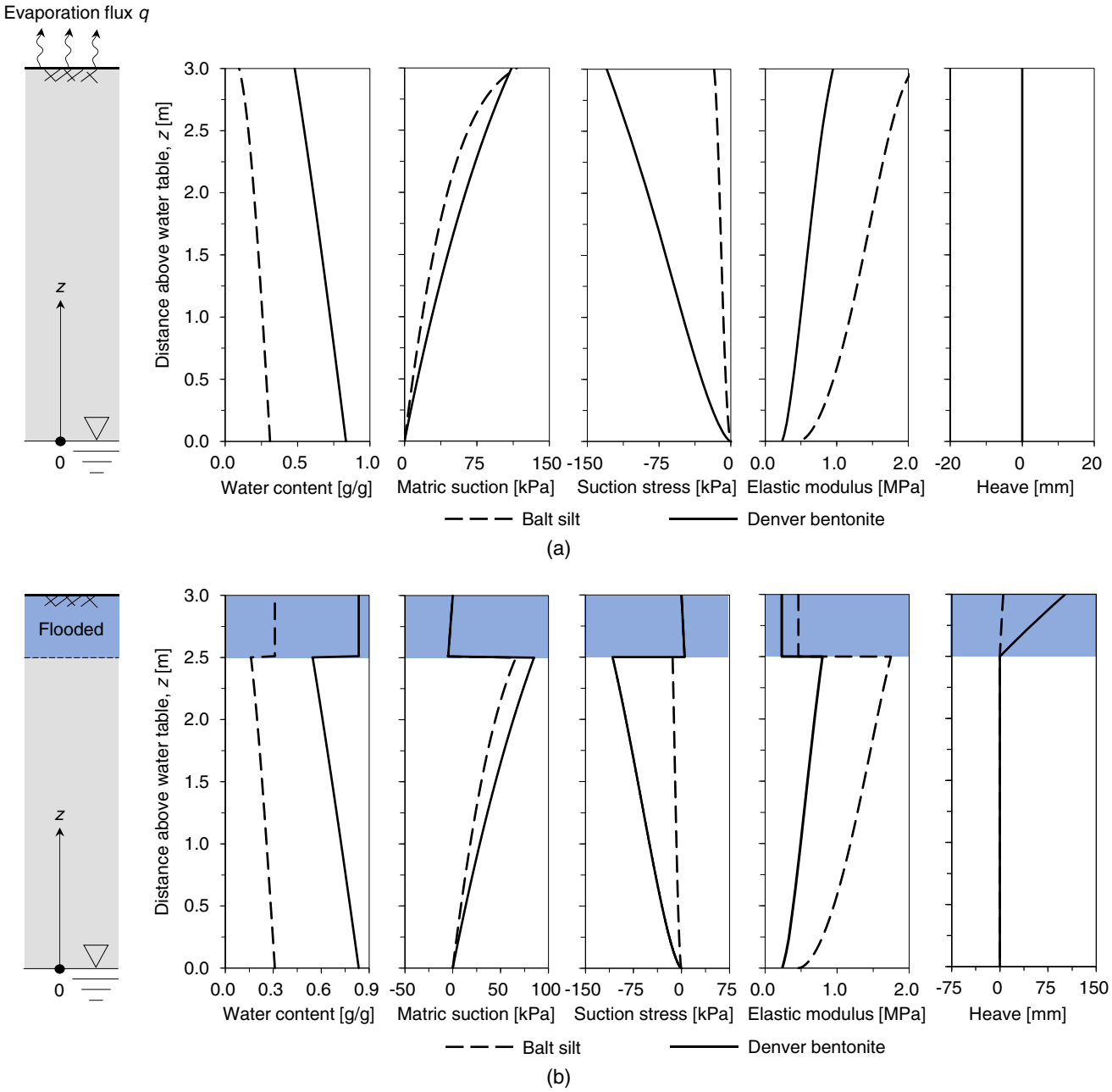

Fig. 10. Estimated water content, matric suction, suction stress, elastic modulus, and heave profiles of a soil layer of the Balt silt and Denver bentonite at: (a) steady state; and (b) flooded state.

$$\Delta h = -\int_{h_0-h_t}^{h_0}\int_{\psi_s}^{\psi_f}\frac{(1+v)(1-2v)}{(1-v)}\mathrm{d}\varepsilon_z(\psi_m, z)\mathrm{d}z \qquad (15)$$

where h_0 = thickness of soil layer (3 m here); h_t = flooded depth (0.5 m); $\mathrm{d}\varepsilon_z$ = the derivative of vertical strain ε_z; z = distance above the water table (3 m below the ground surface); ψ_s = matric suction at steady state (kPa); ψ_f = matric suction at flooded state (kPa); and ψ_m = matric suction (kPa).

To illustrate the impact of elastic modulus's variation, the five soils used earlier to validate the EMCC are used to estimate ground heave with the unified EMCC equation and with a constant elastic modulus E_d by using Eq. (15). The heave profiles for the 3-m layer of the Balt silt and Denver bentonite, respectively, are computed and shown in Fig. 10(b). Table 4 compares the ground heaves estimated with these five soil layers of different elastic modulus (EMCC) and constant elastic modulus (E_d). Generally, the amount of ground heave is consistent with a soil's expansive classification, and the suction stress change dominates the magnitude of ground heave, whereas the total stress change tends to produce negative ground heave, i.e., settlement. For the constant elastic modulus cases, the heaves due to flooding for all five soil layers are marginal: all ≤18.4 mm. For the varying elastic modulus cases, the ground heave becomes significant for more expansive soils, e.g., 5.3 mm for the Balt silt layer, 15.5 mm for the Iowa silt, 20.1 mm for the Missouri clay, 67.2 mm for the Denver claystone, and 101.7 mm for the Denver bentonite. As shown, neglection of elastic modulus variation, i.e., constant elastic modulus, leads to underestimating the ground heaves. Such underestimation increases in terms of the relative displacement as a soil becomes more expansive, e.g., 57.4% for the Iowa silt, 61.7% for the Missouri clay, and 90.9% for the Denver bentonite (Table 4). Therefore, the elastic modulus variation should be considered in

Table 4. Predicted flooding-induced ground displacement of a soil layer with EMCC (Δh_{EMCC}) and constant modulus (Δh_d)

		Ground displacement (+heave, −settlement)				
		Δh_{EMCC} (mm)				
Soil layer	Flooded depth (m)	Total displacement	Induced by total stress	Induced by suction stress	Δh_d (mm)	$(\Delta h_{EMCC} - \Delta h_d)/\Delta h_{EMCC}$ (%)
Balt silt	0.5	5.3	−0.6	5.9	2.3	56.6
Iowa silt	0.5	15.5	−0.4	15.9	6.6	57.4
Missouri clay	0.5	20.1	−1.1	21.2	7.7	61.7
Denver claystone	0.5	67.2	−0.9	68.1	18.4	72.6
Denver bentonite	0.5	101.7	−1.2	102.9	9.3	90.9

geotechnical engineering practice dealing with soil deformation, and the proposed EMCC equation can significantly improve the accuracy of the ground heave estimation.

Summary and Conclusions

A conceptual model has been established to describe the dependence of soil's elastic modulus on water content. It is synthesized that a soil's macroscale elastic modulus depends on two microscale variables, i.e., interparticle stress and interparticle friction coefficient, both of them are controlled by soil-water interaction mechanisms of capillarity and adsorption. Each of the two soil-water interaction mechanisms plays a distinct role in altering the soils' elastic modulus. Adsorptive water tends to penetrate in interparticle contact area and reduces particle-particle attractive forces, thereby reducing the soil's elastic modulus, whereas capillary water increases suction stress or interparticle forces, increasing the soil's elastic modulus.

The proposed conceptual model yields an elastic modulus characteristic curve equation by unifying soil-water interaction effects on the soil's elastic modulus. The unified EMCC equation involves seven physical parameters: two for adsorption (β^E and E_d), four for capillarity (E_{cm}, E_s, w_s, and n^E), and one for both (w^E_{tran}). The unified EMCC equation can explicitly separate adsorptive and capillary elastic modulus and includes cavitation phenomena overlooked by the existing models. It is demonstrated that the unified EMCC can excellently capture the experimental data of the elastic modulus of a wide array of soils, verifying its validity and generality.

The unified EMCC equation is demonstrated to be intrinsically correlated with suction stress characteristic curves and soil shrinkage curves. The unified EMCC equation is implemented to determine suction stress data from soil shrinkage curves. The determined suction stress data can be well represented by the unified effective stress equation with three physical parameters identical to those of the unified EMCC equation, and the unified EMCC and effective stress equations can well predict soil shrinkage data, confirming the ability of the unified EMCC in capturing the elastic modulus's variation.

The practical significance of the proposed EMCC model is illustrated by implementing it in estimating the wetting-induced ground heave/settlement of soil layers. This study shows that the proposed EMCC model can potentially lead to a significant improvement in heave prediction subject to varying moisture conditions.

Appendix I. Determination of Suction Stress from EMCC and Soil Shrinkage Data

Drying induced soil strain under zero external total stress can be expressed as a function of suction stress through Hooke's law:

$$d\varepsilon_v(w) = 3(1-2v)\frac{d\sigma^s(w)}{E(w)} \tag{16}$$

where v = Poisson's ratio; $d\varepsilon_v$ = derivative of volume strain; $d\sigma^s$ = derivative of suction stress (kPa); and $E(w)$ is the elastic modulus characteristic curve equation, expressing the tangent Young's modulus as a function of water content (w). Assuming that the solid volume remains unchanged, the derivative of volume strain $d\varepsilon_v$ is fully contributed by the variation of void volume. Thereby, the derivative of volume strain $d\varepsilon_v$ can be converted to the derivative of void ratio de:

$$d\varepsilon_v = \frac{dV}{V(w)} = \frac{de}{1+e(w)} \tag{17}$$

where V = total soil volume (m^3). Eqs. (16) and (17) can be rewritten as:

$$d\sigma^s = \frac{1}{3(1-2v)}\frac{E(w)}{1+e(w)}de \tag{18}$$

Thereby, the suction stress change $\Delta\sigma^s$ of a soil with water content changing from w_1 to w_2 can be written as:

$$\Delta\sigma^s = \frac{1}{3(1-2v)}\int_{w_1}^{w_2}\frac{E(w)}{1+e(w)}\frac{de}{dw}dw \tag{19}$$

where $e(w)$ can be obtained through linear interpolation of measured soil shrinkage data. For example, the $e(w)$ between soil shrinkage data points (w_1, e_1) and (w_2, e_2) can be written as $e(w) = e_2 + \frac{e_1-e_2}{w_1-w_2}(w-w_2)$.

Appendix II. Prediction of Soil Shrinkage Curves with EMCC and SSCC

The EMCC and SSCC can be combined to predict soil shrinkage curves. Eq. (18) can be expressed as:

$$d\{\ln[1+e(w)]\} = \frac{3(1-2v)}{E(w)}d\sigma^s \tag{20}$$

Integrating Eq. (20) over water content (w), the soil shrinkage curve [e (w)] can be written as follows:

$$e(w) = [e(w_0)+1]\exp\left[\int_{w_0}^{w}\frac{3(2v-1)}{E(w)}\frac{d\sigma^s}{dw}dw\right] - 1 \tag{21}$$

where e_0 and w_0 = initial void ratio and water content, respectively, and w_0 is generally equal to the saturated water content w_s.

Appendix III. Estimation of Heave of a Soil Layer Subjected to Flooding

At the steady state, analytical solutions for water content and matric suction profiles of the soil layer (Fig. 10) are expressed as (Lu and Likos 2004; Lu and Godt 2013):

$$w(z) = w_s \left[\frac{K(z)}{K_s}\right]^{\frac{1}{n}} \tag{22}$$

$$\psi_m(z) = \frac{\rho g}{\beta} \ln\left(\frac{K(z)}{K_s}\right) \tag{23}$$

where K = hydraulic conductivity (m/s) and $K(z) = -q + (q + K_s)e^{-\beta z}$; q = evaporation flux (m/s); K_s = saturated hydraulic conductivity (m/s); ρ = water density (kg/m^3); and g = gravitational acceleration, i.e., 9.8 m/s^2; and β (m^{-1}) and n are fitting parameters. With Eqs. (22) and (23), the water content profile is expressed as a function of matric suction:

$$w(z) = w_s \exp\left[\frac{\beta \psi_m(z)}{\rho g n}\right]$$

The derivative of vertical strain of the soil layer $d\varepsilon_z$ for a homogeneous and isotropic soil layer is expressed as (e.g., Davis and Selvadurai 1996):

$$d\varepsilon_z(\psi_m, z) = \frac{(1+v)(1-2v)}{(1-v)} \frac{d\sigma'(\psi_m, z)}{E(\psi_m, z)} \tag{24}$$

The effective stress σ' is expressed as (e.g., Lu et al. 2010; Zhang and Lu 2020b):

$$\sigma' = \sigma_t - u_a - \sigma^s \tag{25}$$

$$\sigma^s = \begin{cases} \sigma^s(w), & u_a - u_w \geq 0 \\ -(u_a - u_w), & u_a - u_w \leq 0 \end{cases} \tag{26}$$

where u_a = air pressure (kPa); and u_w = pore water pressure (kPa). Eqs. (25) and (26) state that the effective stress σ' can be expressed in terms of suction stress equations (Zhang and Lu 2020b) under both saturated and unsaturated conditions.

Suppose that the top h_t (0.5 m in the example) of the soil layer got saturated under flooding, the ground heave (Δh) is obtained by integrating Eq. (24):

$$\begin{aligned} \Delta h &= -\int_{h_0-h_t}^{h_0} \int_{\psi_s}^{\psi_f} d\varepsilon_z(\psi_m, z) dz \\ &= \underbrace{-\int_{h_0-h_t}^{h_0} \frac{(1+v)(1-2v)}{(1-v)} \frac{\sigma_{t,f}(z) - \sigma_{t,h}(z)}{E_f(z)} dz}_{\text{Total stress component}} \\ &\quad + \underbrace{\int_{h_0-h_t}^{h_0} \int_{\psi_s}^{\psi_f} \frac{(1+v)(1-2v)}{(1-v)} \frac{d\sigma^s(\psi_m, z)}{E(\psi_m, z)} dz}_{\text{Suction stress component}} \end{aligned} \tag{27}$$

where h_0 = thickness of soil layer (3 m here); h_t = flooded depth (0.5 m); $d\varepsilon_z$ = derivative of vertical strain ε_z; z = distance above the water table (3 m below the ground surface); ψ_s = matric suction at steady state (kPa); ψ_f = matric suction at flooded state (kPa); ψ_m = matric suction (kPa); $\sigma_{t,f}$ = total stress at flooded state (kPa); $\sigma_{t,s}$ = total stress at steady state (kPa); and E_f = elastic modulus at flooded state (MPa). The first term on the right-hand side of Eq. (27) represents the settlement due to the increase in the total stress change (flooding), whereas the second term represents the heave/settlement due to the combination of the increase in suction stress and decrease in elastic modulus. The parameters used for the unified EMCC and effective stress equations are listed in Tables 2 and 3.

Data Availability Statement

All data, models, and code generated or used during the study are available from the corresponding author.

Acknowledgments

This research was sponsored in part by the National Natural Science Foundation of China (52078208 and 52090083) to CZ.

References

Akin, I. D., and W. J. Likos. 2014. "Specific surface area of clay using water vapor and EGME sorption methods." *Geotech. Test. J.* 37 (6): 1016–1027. https://doi.org/10.1520/GTJ20140064.

Baker, R., and S. Frydman. 2009. "Unsaturated soil mechanics." *Eng. Geol.* 106 (1–2): 26–39. https://doi.org/10.1016/j.enggeo.2009.02.010.

Banerjee, A., A. J. Puppala, S. S. C. Congress, S. Chakraborty, W. J. Likos, and L. R. Hoyos. 2020. "Variation of resilient modulus of subgrade soils over a wide range of suction states." *J. Geotech. Geoenviron. Eng.* 146 (9): 04020096. https://doi.org/10.1061/(ASCE)GT.1943-5606.0002332.

Butt, H.-J., and M. Kappl. 2018. *Surface and interfacial forces*. 2nd ed. Weinheim, Germany: Wiley-VCH Verlag GmbH.

Chang, C. S., S. S. Sundaram, and A. Misra. 1989. "Initial moduli of particulated mass with frictional contacts." *Int. J. Numer. Anal. Methods Geomech.* 13 (6): 629–644. https://doi.org/10.1002/nag.1610130605.

Culligan, P. J., A. J. Whittle, and J. K. Mitchell. 2019. "The role of geotechnics in addressing new world problems." In *Geotechnical fundamentals for addressing new world challenges*, edited by N. Lu and J. K. Mitchell. Cham, Switzerland: Springer.

Davis, R. O., and A. P. S. Selvadurai. 1996. *Elasticity and geomechanics*. Cambridge, UK: Cambridge University Press.

Dong, Y., and N. Lu. 2017. "Measurement of suction-stress characteristic curve under drying and wetting conditions." *Geotech. Test. J.* 40 (1): 107–121. https://doi.org/10.1520/GTJ20160058.

Dong, Y., N. Lu, and J. S. McCartney. 2018. "Scaling shear modulus from small to finite strain for unsaturated soils." *J. Geotech. Geoenviron. Eng.* 144 (2): 04017110. https://doi.org/10.1061/(ASCE)GT.1943-5606.0001819.

Han, Z., and S. K. Vanapalli. 2016. "State-of-the-art: Prediction of resilient modulus of unsaturated subgrade soils." *Int. J. Geomech.* 16 (4): 04015104. https://doi.org/10.1061/(ASCE)GM.1943-5622.0000631.

Israelachvili, J. N. 2011. *Intermolecular and surface forces*. San Diego: Academic Press.

Khosravi, A., and J. S. McCartney. 2011. "Resonant column test for unsaturated soils with suction–saturation control." *Geotech. Test. J.* 34 (6): 730–739. https://doi.org/10.1520/GTJ103102.

Lu, N. 2008. "Is matric suction a stress variable?" *J. Geotech. Geoenviron. Eng.* 134 (7): 899–905. https://doi.org/10.1061/(ASCE)1090-0241(2008)134:7(899).

Lu, N. 2016. "Generalized soil water retention equation for adsorption and capillarity." *J. Geotech. Geoenviron. Eng.* 142 (10): 04016051. https://doi.org/10.1061/(ASCE)GT.1943-5606.0001524.

Lu, N. 2018. "Generalized elastic modulus equation for unsaturated soil." In *Proc., PanAm Unsaturated Soils 2017: Plenary Papers, Geotechnical Special Publication 300*, 32–48. Reston, VA: ASCE.

Lu, N., and Y. Dong. 2017. "Correlation between soil-shrinkage curve and water-retention characteristics." *J. Geotech. Geoenviron. Eng.* 143 (9): 04017054. https://doi.org/10.1061/(ASCE)GT.1943-5606.0001741.

Lu, N., and J. Godt. 2013. *Hillslope hydrology and stability*. Cambridge, UK: Cambridge University Press.

Lu, N., J. W. Godt, and D. T. Wu. 2010. "A closed-form equation for effective stress in unsaturated soil." *Water Resour. Res.* 46 (5): 1–14. https://doi.org/10.1029/2009WR008646.

Lu, N., and M. Kaya. 2013. "A drying cake method for measuring suction-stress characteristic curve, soil-water-retention curve, and hydraulic conductivity function." *Geotech. Test. J.* 36 (1): 20120097. https://doi.org/10.1520/GTJ20120097.

Lu, N., and M. Kaya. 2014. "Power law for elastic moduli of unsaturated soil." *J. Geotech. Geoenviron. Eng.* 140 (1): 46–56. https://doi.org/10.1061/(ASCE)GT.1943-5606.0000990.

Lu, N., and W. J. Likos. 2004. *Unsaturated soil mechanics*. New York: Wiley.

Lu, N., and W. J. Likos. 2006. "Suction stress characteristic curve for unsaturated soil." *J. Geotech. Geoenviron. Eng.* 132 (2): 131–142. https://doi.org/10.1061/(ASCE)1090-0241(2006)132:2(131).

Lu, N., and C. Zhang. 2019. "Soil sorptive potential: Concept, theory, and verification." *J. Geotech. Geoenviron. Eng.* 145 (4): 04019006. https://doi.org/10.1061/(ASCE)GT.1943-5606.0002025.

Lu, N., and C. Zhang. 2020. "Separating external and internal surface areas of soil particles." *J. Geotech. Geoenviron. Eng.* 146 (2): 04019126. https://doi.org/10.1061/(ASCE)GT.1943-5606.0002198.

Makse, H. A., N. Gland, D. L. Johnson, and L. M. Schwartz. 1999. "Why effective medium theory fails in granular materials." *Phys. Rev. Lett.* 83 (24): 5070–5073. https://doi.org/10.1103/PhysRevLett.83.5070.

Mancuso, C., R. Vassallo, and A. D'Onofrio. 2002. "Small strain behavior of a silty sand in controlled-suction resonant column torsional shear tests." *Can. Geotech. J.* 39 (1): 22–31. https://doi.org/10.1139/t01-076.

McKeen, R. G. 1992. "A model for predicting expansive soil behavior." In *Proc., 7th Int. Conf. on Expansive Soils*, 1–6. New York: ASCE.

Mitchell, J. K., and K. Soga. 2005. *Fundamentals of soil behavior*. New York: Wiley.

Ng, C. W. W., C. Zhou, Q. Yuan, and J. Xu. 2013. "Resilient modulus of unsaturated subgrade soil: Experimental and theoretical investigations." *Can. Geotech. J.* 50 (2): 223–232. https://doi.org/10.1139/cgj-2012-0052.

Or, D., and M. Tuller. 2002. "Cavitation during desaturation of porous media under tension." *Water Resour. Res.* 38 (5): 1–14. https://doi.org/10.1029/2001WR000282.

Poulos, H. G. 1995. "Design of reinforcing piles to increase slope stability." *Can. Geotech. J.* 32 (5): 808–818. https://doi.org/10.1139/t95-078.

Sawangsuriya, A., T. B. Edil, and P. J. Bosscher. 2009. "Modulus-suction-moisture relationship for compacted soils in postcompaction state." *J. Geotech. Geoenviron. Eng.* 135 (10): 1390–1403. https://doi.org/10.1061/(ASCE)GT.1943-5606.0000108.

Schuettpelz, C. C., D. Fratta, and T. B. Edil. 2010. "Mechanistic corrections for determining the resilient modulus of base coarse materials based on elastic wave measurements." *J. Geotech. Geoenviron. Eng.* 136 (8): 1086–1094. https://doi.org/10.1061/(ASCE)GT.1943-5606.0000329.

Zhang, C., Y. Dong, and Z. Liu. 2017. "Lowest matric potential in quartz: Metadynamics evidence." *Geophys. Res. Lett.* 44 (4): 1706–1713. https://doi.org/10.1002/2016GL071928.

Zhang, C., and N. Lu. 2018. "What is the range of soil water density? Critical reviews with a unified model." *Rev. Geophys.* 56 (3): 532–562. https://doi.org/10.1029/2018RG000597.

Zhang, C., and N. Lu. 2019a. "Augmented Brunauer–Emmett–Teller equation for water adsorption on soils." *Vadose Zone J.* 18 (1): 1–12. https://doi.org/10.2136/vzj2019.01.0011.

Zhang, C., and N. Lu. 2019b. "Unitary definition of matric suction." *J. Geotech. Geoenviron. Eng.* 145 (2): 02818004. https://doi.org/10.1061/(ASCE)GT.1943-5606.0002004.

Zhang, C., and N. Lu. 2020a. "Soil sorptive potential: Its determination and predicting soil water density." *J. Geotech. Geoenviron. Eng.* 146 (1): 04019118. https://doi.org/10.1061/(ASCE)GT.1943-5606.0002188.

Zhang, C., and N. Lu. 2020b. "Unified effective stress equation for soil." *J. Eng. Mech.* 146 (2): 04019135. https://doi.org/10.1061/(ASCE)EM.1943-7889.0001718.